PHYSICAL REVIEW LETTERS

Exchange Interaction in the Insulating Phase of $RNiO_3$

J.-S. Zhou, J. B. Goodenough, and B. Dabrowski*

Texas Materials Institute, University of Texas at Austin, 1 University Station, C2201, Austin, Texas 78712, USA
(Received 9 February 2005; published 15 September 2005)

In order to characterize the spin-spin exchange interactions responsible for the Type-E' antiferromagnetic order in inhomogeneous $RNiO_3$ perovskites (R = Y or rare earth), the pressure dependence of the Néel temperature T_N was systematically measured for samples with $T_N < T_{IM}$ and $T_N = T_{IM}$; T_{IM} is an insulator-metal transition temperature. Analysis of the results shows that, as for superexchange, perturbation theory can be used to describe the interatomic exchange interactions for $T_N < T_{IM}$, but the perturbation theory breaks down where T_N approaches T_{IM}.

The theory of superexchange interaction was developed to describe the spin-spin couplings in homogeneous Mott insulators [1]. In the limit of $W/U \ll 1$ where W is the bandwidth and U is the on-site coulomb energy, the explicit expression of the superexchange interaction has been derived by means of the perturbation method. Efforts to explore the evolution of the superexchange interaction as the crossover to itinerant electronic behavior is approached from the localized-electron side can be tracked back to a half century ago [2]. This initiative faded away for lack of a system where the crossover could be stabilized. A reversal of the sign of dT_N/dP was proposed by one of the authors assuming that the system remains homogeneous over the transition from localized to itinerant electronic behavior [3]. Extensive research on transition-metal oxides over the last two decades reveals that phase segregation commonly occurs at the crossover. A large body of literature on this phenomenon can be found for the mixed-valent systems of superconductive cuprates and magnetoresistive manganites. The $RNiO_3$ family is a single-valent system in which a complete evolution from a Pauli paramagnetic metal to a Curie-Weiss insulator can be achieved by applying chemical pressure, i.e., by rare-earth substitution. Transition temperatures are illustrated in Fig. 1 as a function of the ionic radius (IR) of the rare-earth ion. Hydrostatic pressure has been found to influence the insulator-metal transition temperature T_{IM} in a manner similar to increasing the IR. More importantly, pressure provides a fine tuning of the lattice parameter, which allows one to explore the phase evolution at crossover in great detail. Accessibility to the phase changes at crossover by chemical and hydrostatic pressure makes $RNiO_3$ an ideal system to study the exchange interaction where the W/U ratio is not small.

Similar to the mixed-valent systems at crossover, the local structure in the insulator phase of the $RNiO_3$ perovskites near T_{IM} is more complicated than in a Mott insulator. Fast probes such as resonant x-ray scattering (RXS) [4,5] and x-ray-absorption fine structure (EXAFS) [6] have been used to characterize the local structure. Although it could be simply a technical issue to resolve the possible bond length segregation below T_{IM} in the light rare-earth

$RNiO_3$, the segregation found by using RXS in $NdNiO_3$ [4] is significantly smaller than that in the $RNiO_3$ (R = Y, Ho, ... Lu) where the static segregation into ionic and covalent Ni-O bonds takes place [7]. Moreover, the giant oxygen isotope effect on T_{IM} [8] indicates that the oxygen motion involving bond length segregation remains dynamic in the light rare-earth $RNiO_3$. On the other hand, neutron diffraction at room temperature, which gives averaged atomic positions, shows [see Fig. 1(b)] that the Ni-O bond length 1.94 Å $< d_{Ni-O} <$ 1.96 Å for the insulator phase of $RNiO_3$ (R = Sm, Eu, ... Dy) remains much smaller than the ionic Ni-O bond ($\sim$2.00 Å) which has
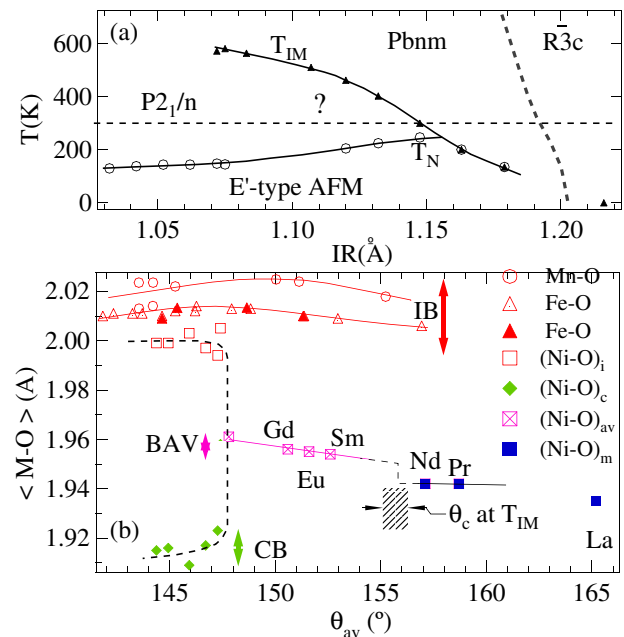
FIG. 1 (color online). (a) The phase diagram of critical temperatures vs the R^{3+}-ion radius (IR); (b) the M-O bond length and M-O-M bond angle for RMO_3 at room temperature; see Ref. [7] for a list of data sources. The Mn-O bond length is the average value of three ionic bonds. IB is ionic bond length; BAV is the averaged bond length of $RNiO_3$; CB is covalent bond length for $RNiO_3$.

been identified in the $RNiO_3$ compounds ($R = Y$, Ho, ...Lu) and other perovskite insulators. Although an inhomogeneous local structure has been found in the insulator phase, sharp and well-defined insulator-metal transition T_{IM} and the Néel temperature T_N have been found to be closely related to the Ni-O bond length and the ($180° - \phi$) Ni-O-Ni bond angle as determined by neutron diffraction, which allows us to demonstrate a relationship between T_N and the bandwidth W. Even though the behavior of T_{IM} under hydrostatic pressure has been reported by many groups [9–13], a systematic measurement of T_N under pressure in the insulator phase is not available in part due to the difficulty of probing a weak signal from spin ordering in the family. We have been able to monitor $T_N(P)$ as shown in this work. $T_N(P)$ as well as $T_N(W)$ created by using data in the literature demonstrate how the superexchange interaction evolves as the perturbation expansion breaks down on the approach to crossover.

We use an anomaly in the resistivity $\rho(T)$ at T_N to track the pressure dependence of T_N. However, the anomaly at $T_N < T_{IM}$ is too weak to be discerned unambiguously in normally prepared ceramic samples. Therefore, we used the cold-press technique we developed previously [14] to obtain high-density ceramic samples of $RNiO_3$ ($R = $ La, ... Gd). The pellets were cut with a diamond saw into rectangular $0.5 \times 0.5 \times 2.5$ mm bars. The contact spots on the sample surface were prepared by cold melting of metallic indium before Cu wires were pressed on with small pieces of In foil. With this method, the contact resistance is less than 1 Ω, which is much lower than that for contacts made with heat-treated silver epoxy on these samples. With these procedures, the significantly high-quality $\rho(T)$ data of Fig. 2 were obtained. The magnitude of the resistivity obtained with these samples is
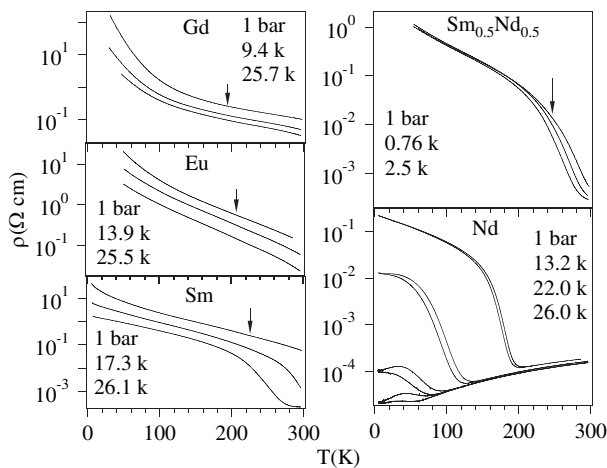
lower than that of a single-crystal film for the corresponding $RNiO_3$ compound. The setup for measuring $\rho(T)$ under pressure has been described elsewhere [11] and the measurement of magnetic susceptibility was carried out in a SQUID magnetometer (Quantum Design). The members of the $RNiO_3$ family were selected to cover phases with Néel temperatures $T_N < T_{IM}$ and $T_N = T_{IM}$.

A monotonic decrease of T_{IM} with pressure and with increasing radius of the R^{3+} ion is clearly visible in Fig. 2. The insulator-metal transition at T_{IM} stays well above room temperature in $EuNiO_3$ and $GdNiO_3$, but it falls down to 280 K in $SmNiO_3$ under a pressure $P = 28$ kbar and below 50 K at 26 kbar in $NdNiO_3$. However, no obvious anomaly in $\rho(T)$ can be seen at the $T_N < T_{IM}$ determined from the magnetic susceptibility for $R = Sm_{0.5}Nd_{0.5}$, Sm, Eu, and Gd. In contrast, spin ordering creates a remarkable anomaly in $\rho(T)$ of the Mott insulators $LaTiO_3$ [15] and $LaVO_3$ [16]. Spin ordering normally alters the energy gap of a magnetic insulator; therefore, the anomaly in derivative $F = d\ln\rho/d(1/T)$ is widely used to track a magnetic transition temperature. As illustrated in Fig. 3, the function $F(T)$ exhibits clearly an anomaly at the T_N of $SmNiO_3$ as determined by the inverse susceptibility. However, the transition temperature can be defined more precisely by the sharp minimum of dF/dT; this more precise definition was used to track the pressure dependence of T_N for our $RNiO_3$ samples.

Figure 4 shows the pressure dependence of T_N for the $RNiO_3$ samples. For $R = Gd$, Eu, and Sm, T_N increases linearly with pressure and dT_N/dP increases with the size of the R^{3+} ion. However, the largest dT_N/dP, which is found for $R = Sm$, is restricted to $P < 15$ kbar; at higher pressures, dT_N/dP drops sharply to near zero. $Sm_{0.5}Nd_{0.5}NiO_3$ has its T_N close to T_{IM} as can be seen in Fig. 1, and a moderate pressure $P \geq 3$ kbar makes T_{IM} overlap T_N. Observations of a pressure-independent T_N for $P \leq 3$ kbar in this composition and the change of dT_N/dP under $P \geq 15$ kbar in $SmNiO_3$ reflect how T_N approaches to T_{IM}. It should be noted that the insulator-metal transition at T_{IM} creates a large change in $F(T)$ near T_{IM}, which

FIG. 2. Typical temperature dependence of the resistivity under pressure for $RNiO_3$. Arrows indicate T_N at ambient pressure. Pressures correspond to the $\rho(T)$ curve from top to bottom.
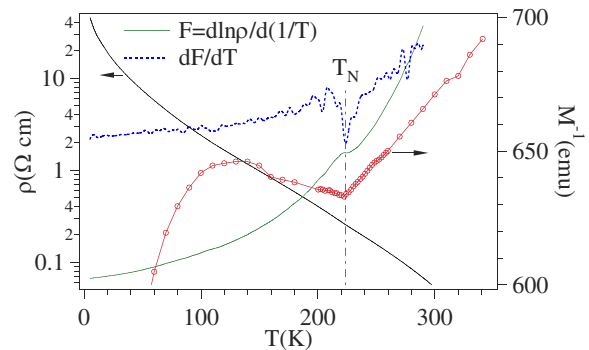
FIG. 3 (color online). Temperature dependence of the resistivity ρ, inverse magnetization M^{-1}, the function $d\ln\rho/d(1/T)$, and its derivative for $SmNiO_3$ at ambient pressure.
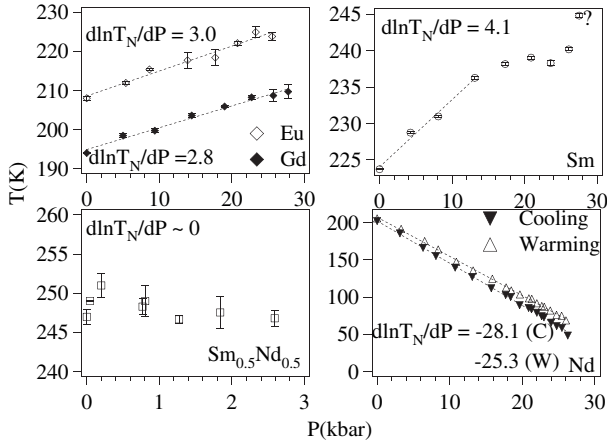
FIG. 4. The pressure dependence of T_N for $RNiO_3$ ($R = Nd_{0.5}Sm_{0.5}$, Sm, Eu, Gd) and of T_N/T_{IM} for $NdNiO_3$. The unit of $d\ln T_N/dP$ is 10^{-3} $(kbar)^{-1}$.

makes the anomaly in $F(T)$ at $T_N < T_{IM}$ diminish to the noise level as T_N approaches T_{IM}. Therefore, the T_N obtained for $SmNiO_3$ at highest pressure may reflect an interference from the $F(T)$ anomaly at T_{IM}. On the other hand, it should be pointed out that the plateau in T_N versus P for $SmNiO_3$ is lower than that in $Sm_{0.5}Nd_{0.5}NiO_3$ by a $\Delta T_N \approx 10$ K. This observation could indicate that T_{IM} is more sensitive to hydrostatic pressure with a single A-site cation than with disordered $R_{1-x}R'_x$. Pressure lowers T_{IM} of $SmNiO_3$ significantly so that it makes T_N saturate at a relatively low temperature. As is also shown in Fig. 4 for $NdNiO_3$, $T_{IM} = T_N$ decreases with hydrostatic pressure, and the hysteresis $\rho(T)$ at T_{IM} indicates that the first-order character becomes more pronounced as $T_{IM} = T_N$ decreases below 200 K.

Since T_N is clearly related to the bond length and angle determined from neutron diffraction as shown in Fig. 1, it is useful to check whether models for a homogeneous phase are applicable to results presented in Fig. 4. In order to extract the bandwidth dependence of the magnetic-exchange interaction from the pressure dependence of T_N, we introduce the Bloch rule [17]. This empirical rule relates dT_N/dP and the volume compressibility $d\ln V/dP$; the Bloch rule $\alpha_B \equiv (d\ln T_N/dP)/(d\ln V/dP) \approx -3.3$ has been found to hold for most antiferromagnetic insulators. The Néel temperature T_N is proportional to the nearest-neighbor spin-spin exchange interactions,

$$T_N \sim J \sim b^2[U^{-1} + (2\Delta)^{-1}], \tag{1}$$

where the electron-energy transfer integral b enters the tight-binding bandwidth $W = 12b$. The critical assumption to make the Bloch rule applicable is that the on-site Coulomb energy U and the charge-transfer gap Δ entering the expression for the superexchange and semicovalent-exchange interactions remain constant under pressure. The assumption appears to be violated in $LaMnO_3$ where an

anomalously high $|\alpha_B|$ was found [18]. In contrast, the Bloch rule holds roughly for isostructural $RMnO_3$ ($R = $ Pr, Sm) [19] where a further reduction in the Mn-O-Mn bond angle enlarges $W_c - W$, where W_c is the critical bandwidth for crossover.

The bandwidth dependence of T_N in an orthorhombic perovskite can be obtained by using the first-order approximation [20] $W \sim \cos\omega/(\text{Ni-O})^{3.5}$ where the definition of the angle ω is shown in Fig. 5. This approximation has been applied by Medarde *et al.* [21] in the case of $PrNiO_3$. High-resolution neutron-diffraction data [22–26] on the $RNiO_3$ family make possible the new phase diagram of transition temperatures versus W or W^2. A relatively small change of the bandwidth for the whole family of $RNiO_3$ perovskite makes the plots of T_N versus W and versus W^2 similar. However, the latter plot is shown in Fig. 5 in order to test the relationship of Eq. (1). We highlight two important features of this phase diagram: (1) T_N varies linearly with the square of the bandwidth, W^2, for the $RNiO_3$ perovskites having $T_N < T_{IM}$ and (2) although the absence of structural data for $Sm_{0.5}Nd_{0.5}NiO_3$ makes us tentatively place its T_N and T_{IM} on linear extrapolations from the other insulators of $RNiO_3$ ($R = $ Sm, Eu, Gd), the change in W^2 from the insulator phase of $Sm_{0.5}Nd_{0.5}NiO_3$ to metallic $NdNiO_3$ is significantly greater than that found for similar R^{3+}-ion changes either among the insulator compositions or the metallic compositions within the orthorhombic phase. A large gap of W^2 between the insulator phase and the metallic phase corresponds to an unusually low bulk module in $Nd_{0.5}Sm_{0.5}NiO_3$ [27]. Moreover, in light of Fig. 5, it becomes necessary to reevaluate phase diagrams for systems exhibiting a transition from localized to itinerant electronic behavior.

The linear relationship of T_N versus W^2 in Fig. 5 for the magnetic insulator phase of $RNiO_3$ ($R = $ Sm, Eu, Gd) is accounted for qualitatively by Eq. (1), which was obtained
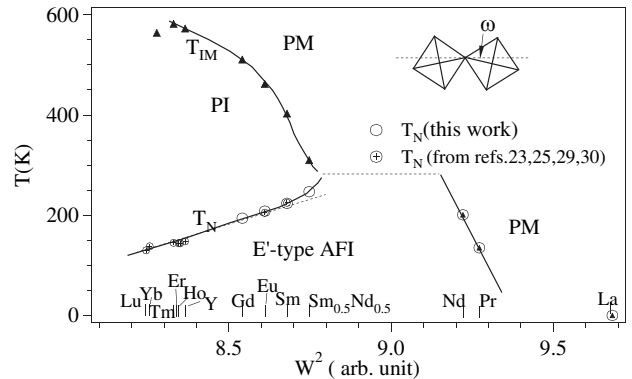
FIG. 5. The phase diagram of transition temperatures vs bandwidth W^2 at room temperature. T_{IM} and T_N are taken from Refs. [23,25,29,30]. Lines inside the figure are guides to the eyes. Inset: definition of the angle ω used to obtain $W \sim \cos\omega/(\text{Ni-O})^{3.5}$.

from higher-order perturbation theory, since the tight-binding theory gives $W \sim b$. The large uncertainty in determining the volume compressibility of $RNiO_3$ makes it difficult to check the Bloch rule. However, the magnitude of $d \ln T_N/dP$, a dominate factor in the Bloch coefficient, falls into a range 2.1–2.5×10^{-3} $(kbar)^{-1}$ for ionic magnetic insulators [14]. Therefore, the $d \ln T_N/dP = 2.8 \times 10^{-3}$ $(kbar)^{-1}$ and 3.0×10^{-3} $(kbar)^{-1}$ found in $GdNiO_3$ and $EuNiO_3$ of Fig. 3, respectively, confirms *quantitatively* that the Bloch rule holds marginally for the insulators $RNiO_3$ given a constant compressibility $\kappa \approx 0.68$ $(kbar)^{-1}$ holds for a wide range of magnetic insulators [14]. The high population of ionic bonds in the insulator phase with $T_{IM} > T_N$ appears to play an important role to keep U from collapsing globally. The remarkable increase of $d \ln T_N/dP$ to 4.11×10^{-3} $(kbar)^{-1}$ found in $SmNiO_3$, however, may signal a reduced U in the framework of the perturbation formula, a change that reflects the approach to crossover from the insulator phase to the metallic phase. The $d \ln T_N/dP \approx 0$ found in $Sm_{0.5}Nd_{0.5}NiO_3$ and in $SmNiO_3$ under $P > 15$ kbar is absolutely not justified by the perturbation theory. As a matter of fact, a clear deviation of T_N in $Sm_{0.5}Nd_{0.5}NiO_3$ from the linear relationship shown in Fig. 5 supports the conclusion that the perturbation formula breaks down at a composition between $SmNiO_3$ and $Sm_{0.5}Nd_{0.5}NiO_3$. On the other hand, a giant magnitude of $d \ln T_N/dP = -281 \times 10^{-3}$ $(kbar)^{-1}$ for $NdNiO_3$ reflects a discontinuous volume change at $T_N = T_{IM}$. This value is comparable to that obtained previously [9].

These observations lay down some guidelines for understanding the electronic state of $RNiO_3$. By using photoemission spectroscopy, Vobornik *et al.* [28] have demonstrated a sharp difference in the spectral properties between the insulator phase with $T_{IM} > T_N$ and that with $T_{IM} = T_N$. The spectral weight is transferred continuously from the Fermi energy to higher binding energy on lowering the temperature through T_{IM} for the phase with $T_{IM} = T_N$ whereas it has no change for the phase with $T_{IM} > T_N$. A sharp difference of dT_N/dP between the phase with $T_N < T_{IM}$ and the phase with $T_N = T_{IM}$ is consistent with the photoemission results. More importantly, a dramatic change of $T_N(P)$ near the phase boundary reveals how the electronic state evolves at the crossover, i.e., $T_N = T_{IM}$. The isotope effect on T_{IM} is another parameter used to characterize the two phases. A giant coefficient $d \ln T_{IM}/d \ln M$ for the phase with $T_{IM} = T_N$ suggests that electron coupling to lattice vibrations may be an important factor causing the perturbation theory to break down as $T_N = T_{IM}$ is approached under pressure from the phase with $T_N < T_{IM}$.

In conclusion, the insulator phase in $RNiO_3$ is not a classic Mott insulator, but an inhomogeneous phase that has been characterized by neutron diffraction, RXS, and EXAFS. Models such as the perturbation theory of the superexchange interaction and the Bloch rule for the ho-

mogeneous system have been shown to be nearly fulfilled in the inhomogeneous magnetic insulator phase. As the insulator-metal transition is approached, the phase shows a much steeper pressure dependence of $T_N(P)$ than predicted by the Bloch rule that is followed by a pressure-independent T_N. These findings place a clear constraint on models describing the evolution of the superexchange interaction at the crossover from localized to itinerant electronic behavior at least in the case of a perovskite with an orbital degeneracy.

*Also at: Department of Physics, Northern IL University, FW 216, DeKalb, IL 60115.
 [1] P. W. Anderson, in *Magnetism*, edited by G. T. Rado and H. Suhl (Academic, New York, 1963), Vol. 1, p. 25.
 [2] N. F. Mott, *Metal-Insulator Transitions* (Taylor & Francis, London, 1990).
 [3] J. B. Goodenough, J. M. Longo, and J. A. Kafalas, Mater. Res. Bull. **3**, 471 (1968).
 [4] U. Staub *et al.*, Phys. Rev. Lett. **88**, 126402 (2002).
 [5] J. E. Lorenzo *et al.*, Phys. Rev. B **71**, 45128 (2005).
 [6] C. Piamonteze *et al.*, Phys. Rev. B **71**, 12104 (2005).
 [7] J.-S. Zhou and J. B. Goodenough, Phys. Rev. B **69**, 153105 (2004).
 [8] M. Medarde *et al.*, Phys. Rev. Lett. **80**, 2397 (1998).
 [9] X. Obradors *et al.*, Phys. Rev. B **47**, 12353 (1993).
[10] P. C. Canfield *et al.*, Phys. Rev. B **47**, 12357 (1993).
[11] J.-S. Zhou *et al.*, Phys. Rev. B **61**, 4401 (2000).
[12] J. L. Garcia-Munoz *et al.*, Phys. Rev. B **69**, 94106 (2004).
[13] R. Lengsdorf *et al.*, J. Phys. Condens. Matter **16**, 3355 (2004).
[14] J.-S. Zhou, J. B. Goodenough, and B. Dabrowski, Phys. Rev. B **67**, 20404 (2003).
[15] Y. Okada *et al.*, Phys. Rev. B **48**, 9677 (1993).
[16] S. Miyasaka, T. Okuda, and Y. Tokura, Phys. Rev. Lett. **85**, 5388 (2000).
[17] D. Bloch, J. Phys. Chem. Solids **27**, 881 (1966).
[18] J.-S. Zhou and J. B. Goodenough, Phys. Rev. Lett. **89**, 87201 (2002).
[19] J.-S. Zhou and J. B. Goodenough, Phys. Rev. B **68**, 54403 (2003).
[20] W. A. Harrison, *The Electronic Structure and Properties of Solids* (Freeman, San Francisco, 1980).
[21] M. Medarde *et al.*, Phys. Rev. B **52**, 9248 (1995).
[22] J. A. Alonso *et al.*, Phys. Rev. Lett. **82**, 3871 (1999).
[23] J. A. Alonso *et al.*, J. Am. Chem. Soc. **121**, 4754 (1999).
[24] J. A. Alonso *et al.*, Phys. Rev. B **61**, 1756 (2000).
[25] J. A. Alonso *et al.*, Phys. Rev. B **64**, 94102 (2001).
[26] J. L. Garcia-Munoz *et al.*, Phys. Rev. B **46**, 4414 (1992).
[27] J.-S. Zhou, J. B. Goodenough, and B. Dabrowski, Phys. Rev. B **70**, 81102 (2004).
[28] I. Vobornik *et al.*, Phys. Rev. B **60**, R8426 (1999).
[29] J. B. Torrance *et al.*, Phys. Rev. B **45**, 8209 (1992).
[30] M. L. Medarde, J. Phys. Condens. Matter **9**, 1679 (1997).